CHEMISTRY
A EUROPEAN JOURNAL

DOI: 10.1002/chem.200800814

Light-Driven Rotary Molecular Motors on Gold Nanoparticles

Michael M. Pollard, Matthijs K. J. ter Wiel, Richard A. van Delden, Javier Vicario, Nagatoshi Koumura, Coenraad R. van den Brom, Auke Meetsma, and Ben L. Feringa*[a]

Abstract: We report the synthesis of unidirectional light-driven rotary molecular motors based on chiral overcrowded alkenes and their immobilisation on the surface of gold nanoparticles through two anchors. Using a combination of ^{1}H and ^{13}C NMR, UV/Vis and CD spectroscopy, we show that these motors preserve their photochemical and thermal behaviour after they have been attached to gold nanoparticles. Furthermore, we describe the synthesis of ^{2}H- and ^{13}C-labelled derivatives that were used to verify the unidirectionality of the rotary cycle of these motors both in solution and while grafted to gold nanoparticles. Taken together, these data support the conclusion that these motors maintain their unidirectional rotary cycle when grafted to the surface of small (ca. 2 nm) gold nanoparticles. Thus, continuous irradiation of the system under appropriate conditions leads to unidirectional rotation of the upper half of the molecules relative to the entire nanoparticle.

Keywords: circular dichroism · molecular devices · nanostructures · nanotechnology · photochemistry

Introduction

Controlled manipulation of matter on the nanoscale by means of molecular machines has been identified as one of the most challenging frontiers of nanotechnology.[1] To be able to do this, chemists must develop molecular systems that can perform mechanical tasks in an environment that is continuously overwhelmed by Brownian motion.[2,3] In an effort to gain control over motion at the molecular scale, several designs of linear and rotary molecular motors have been reported.[3–9] While most of these operate exclusively in solution, it is anticipated that anchoring molecular motors to surfaces is an essential step toward transmitting their actions into work upon their surrounding environment. Indeed, anchoring linear motors to surfaces has enabled the fabrication of more complex molecular devices that can perform mechanical work.[10] Synthetic rotary molecular motors characterized on surfaces, however, are much more scarce.[3a,b,11,13]

Biological systems use rotary molecular motors in a diverse array of key cellular functions including cellular translocation, ion pumping, and ATP biosynthesis.[12] In all of these capacities, one "stator" half of the biomotor is immobilized within a cell membrane, so that the cell can harness the rotary motion of the "rotor".

The designs of these complex natural systems inspired us to explore the effect of immobilizing light-driven rotary molecular motors on surfaces. We found that the rotation of the upper half relative to the lower half of the molecule in solution could be converted to absolute rotation of the upper half relative to a gold nanoparticle.[13] We report the synthesis and characterisation of motors on small (ca. 2 nm) gold colloidal particles. Using UV, CD and NMR spectroscopy, we compared each of the photochemical and thermal steps of the rotary cycle of the light-driven rotary motors attached to the surface of gold nanoparticles to the analogous steps of the parent molecule operating in solution. From this comparison, we show that the photochemical and thermal steps of the unidirectional rotary cycle of the motor are preserved when the molecules are grafted onto the nanoparticles.

Molecular design: One of the most promising designs of rotary molecular motors is based on overcrowded alkenes (exemplified by **1** in Figure 1 and **3** in Figure 2). As shown

[a] Prof. Dr. M. M. Pollard, Dr. M. K. J. ter Wiel, Dr. R. A. van Delden, Dr. J. Vicario, Dr. N. Koumura, Dr. C. R. van den Brom, Dr. A. Meetsma, Prof. Dr. B. L. Feringa
Department of Organic and Molecular Inorganic Chemistry
Stratingh Institute for Chemistry, University of Groningen
Nijenborgh 4, 9747 AG Groningen (The Netherlands)
Fax: (+31) 50-363-4296
E-mail: b.l.feringa@rug.nl

Supporting information for this article is available on the WWW under http://dx.doi.org/10.1002/chem.200800814.

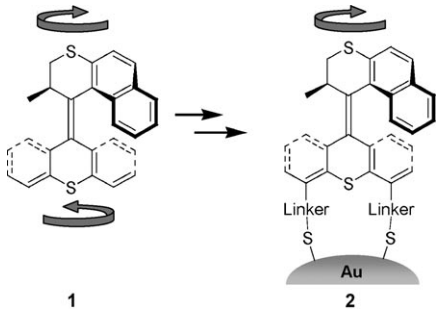

Figure 1. Translation of unidirectional rotary motion in solution into absolute rotary motion is achieved by grafting the stator half of the motor to a gold nanoparticle.

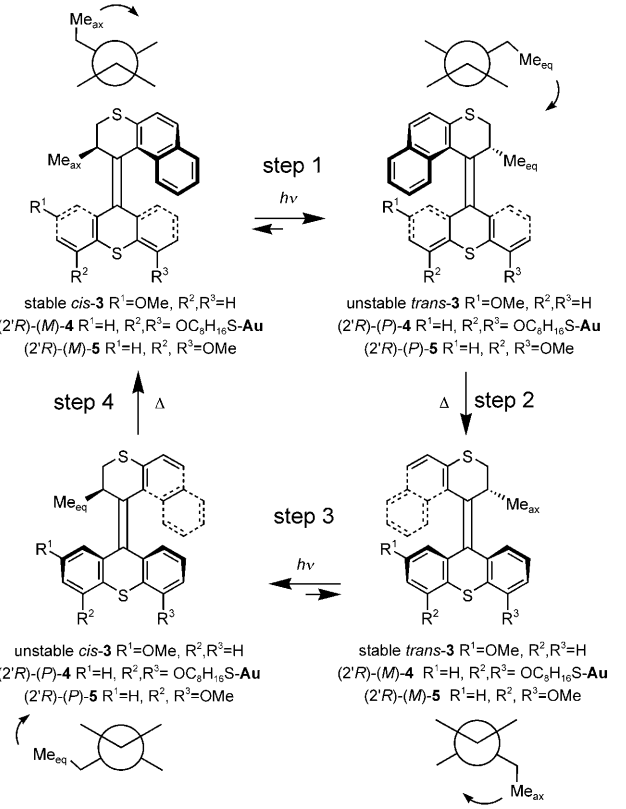

Figure 2. Rotary cycle of **3**, **4** and **5**, with illustrative Newman projections along the central olefinic bond.[14]

in Figure 2, in the stable isomers of **3** a single stereogenic centre bearing a methyl group dictates the direction of rotation. This methyl group adopts a pseudo-axial position to minimize steric strain with the adjacent aromatic moiety in the lower half. The motor functions as follows: absorption of a photon (energy input) leads to *cis*→*trans* isomerisation of the central overcrowded alkene, the axis of rotation of the motor. This isomerisation leaves the molecule in a high-energy state in which the methyl group occupies a pseudo-equatorial position, where it experiences steric crowding with the lower half of the molecule. A thermodynamically favourable helix inversion relieves the strain, as both the methyl group and the naphthalene ring slip past the aromatic moieties of the lower half. This rate-limiting step regenerates the stable isomer in which the methyl substituent is in a pseudo-axial position, and thus 180° rotation of the upper half relative to the lower half has occurred. Repeated photoisomerisation followed by helix inversion results in continual unidirectional rotation. Upon constant irradiation at appropriate temperatures that allow facile thermal helix inversion, the upper half of the molecule undergoes continual unidirectional rotation relative to the lower half. The speed of rotation can be adjusted by replacing the sulfur atoms in **3** with oxygen and carbon.[6b,8]

Attaching the motor appropriately to a solid support transforms the relative rotary motion of the upper half with respect to the lower half into absolute rotary motion relative to the support. The use of gold colloids as solid support is attractive because their synthesis is relatively straightforward[15] and well precedented, and because photochemical reactions of molecules in monolayers on gold nanoparticles are also known.[16,17] Moreover, the motor-decorated nanoparticles can be easily studied by UV/Vis and CD spectroscopy. This is essential for following each step of the rotary cycle and evaluating the effect, if any, that immobilisation has on either the photochemical or thermal steps in the rotary cycle.

In the design, it was essential that the motor molecule be attached to the nanoparticle through two points to prevent Brownian rotation around single bonds. The tethers should be long enough to allow sufficient conformational flexibility and, more importantly, to permit photoisomerisation of the motor with minimal interference/quenching by the gold nanoparticle. For these reasons an eight-carbon chain was chosen.[17] Moreover, the choice of a longer tether would avoid overcrowding of the motor molecules around the gold core of the particle, which could influence both the photochemical and thermal steps of the rotary cycle.

To facilitate complete characterisation of the different states of the molecule through its four-step rotary cycle, the motor was designed to be similar in structure to reported slow motor molecules.[8] The reported half-life for the rate-limiting thermal isomerisation step in the rotary cycle of **1** at room temperature is 215 h,[6] which suggests that the unstable isomers of **3** could be easily characterized at room temperature. We anticipated that using CD spectroscopy would make it possible to evaluate the photoequilibria and rates of thermal isomerisation.

Retrosynthesis: There are three major aspects to consider in the retrosynthesis of our motor-functionalized gold nanoparticle (Scheme 1). First, the motor molecule needs two tethers for attachment to the gold nanoparticle. Since each tether contains an oxygen-sensitive thiol group, it is must be attached at a late stage of the synthesis, preferably on a deprotected form of model motor molecule **5**. Second, we anticipated that the key step in the synthetic sequence would be the Barton–Kellogg coupling reaction,[18,19] because this method introduces the steric strain gradually over three con-

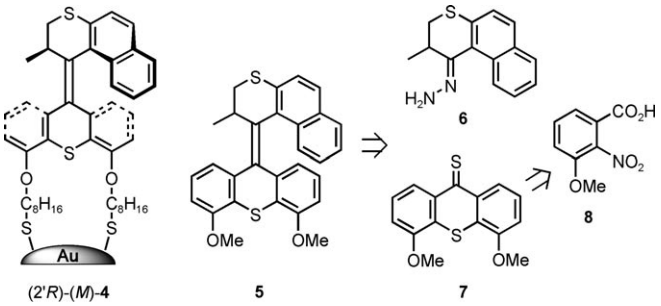

Scheme 1. Retrosynthesis of surface-bound molecular motor (2′*R*)-(*M*)-**4**.

secutive steps starting from high-energy intermediates. The precursors required for the Barton–Kellogg reaction are the known hydrazone **6** and a thioketone of lower half **7**. Although the synthesis of this thioketone initially appears relatively easy, since it involves only well-established manipulations of aromatic functional groups, it requires an 1,2,3-substitution pattern in one of its building blocks.

Finally, enantiomerically pure material is needed to demonstrate unidirectionality of rotary motion of the motor anchored to the gold nanoparticle. The motor molecule must be resolved by chiral HPLC at some stage of the synthesis. This resolution is preferably performed at a late stage of the synthesis to minimize the number of transformations that must be performed on enantiomerically pure material. We envisioned that the retrosynthesis shown in Scheme 1 addresses the key criteria mentioned above for a functional motor on the surface of a nanoparticle.

Results and Discussion

Synthesis of parent motor 5: Synthesis of thioketone **7**, required for the lower half, is deceptively challenging because of the 1,2,3-substitution pattern in one of the necessary arene building blocks. Synthesis of the lower half of the molecule started with 3-methoxy-2-nitrobenzoic acid (**8**), which was reduced to aniline **9** in a hydrogen atmosphere with palladium on carbon (Scheme 2). A Sandmeyer-type reaction[20] sequence provided an impure sample of 2-iodo-3-methoxybenzoic acid (**11**) which was purified after esterification with methyl iodide to give methyl ester **10**. Saponification regenerated acid **11**, which was then subjected to classical Ullmann conditions[21] with copper powder and potassium carbonate in DMF at high temperatures in the presence of 2-methoxybenzenethiol to give aryl thioether **14**. As purification of the carboxylic acid product was complicated by formation of side products, methyl iodide was added to the cooled reaction mixture to allow isolation of methyl ester **13** in acceptable yields. The acid functionality was restored by saponification of the ester with lithium hydroxide, which was followed by ring closure in polyphosphoric acid (PPA) to give ketone **15**. In analogy with a procedure used by Vasiliu and co-workers on a ketone of similar structure,[22] treatment of **15** with phosphorus pentasulfide in toluene at reflux

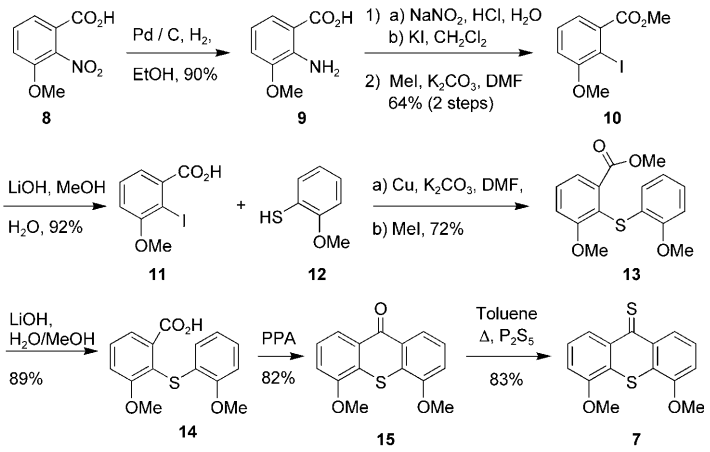

Scheme 2. Initial synthesis of the thioxanthone lower half with two methoxyl groups amenable to further functionalisation.

yielded thioketone **7** in 83% yield as a dark green solid. In summary, this approach required ten chemical transformations to obtain thioketone **7** in 27% overall yield.

Despite the fact that this multistep sequence included several difficult purifications, as well as steps with modest yields, it was suitable to initially obtain moderate amounts of parent motor **5**. We subsequently sought a shorter, more efficient route to provide a larger amount of material for study, in particular for use in the synthesis of the desymmetrized ^{13}C-labelled motor. A more convenient route was developed which employs the Snieckus anionic equivalent of the Friedel–Crafts cyclisation (Scheme 3).[23]

In the first step, 3-methoxybenzoic acid (**17**) was converted to amide **18** via its acid chloride followed by treatment with diethylamine in the presence of triethylamine.[24] The *ortho*-lithiation of amide **18** was described previously by Beak and Brown, and proceeded well with a complex of *sec*-butyllithium and *N*,*N*,*N*′,*N*′-tetramethylethylenediamine (TMEDA).[25] In situ treatment of lithium species **19** with disulfide **16**[26] gave thioether **20** in 84% yield. Subsequent treatment of this amide with lithium diisopropylamide

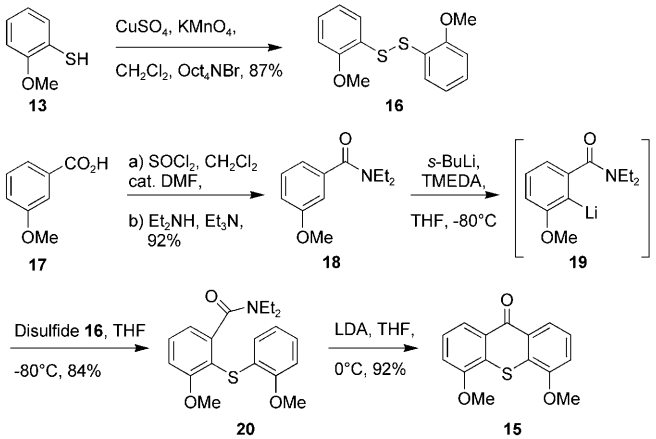

Scheme 3. Improved route towards lower-half ketone **16** by using the Snieckus anionic Friedel–Crafts cyclisation.[23]

(LDA) resulted in cyclisation to afford the key ketone **15** in high yield.[27] This new synthetic route conveniently provides ketone **15** in only three steps in an overall yield of 71%.

Thioketone **7** was then used in the key step in the synthesis of the motor molecule (Scheme 4): introduction of the

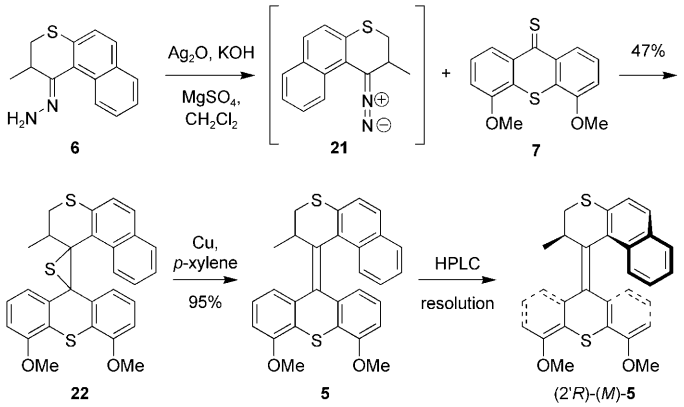

Scheme 4. Final steps to parent motor molecule **5** by a Barton–Kellogg reaction sequence, followed by resolution by HPLC on a chiral stationary phase.

central olefin through a Barton–Kellogg reaction sequence.[18,19] Although several protocols for the formation of sterically overcrowded alkenes have been developed,[28] advantages of the Barton–Kellogg reaction include the possibility to selectively form unsymmetrical alkenes by using two distinct building blocks, and the gradual increase in steric strain in the molecule through several highly exothermic steps. These steps begin with a 1,3-dipolar cycloaddition, followed by ring contraction from a five- to a three-membered ring with extrusion of N_2, and finally extrusion of sulfur to give the olefin.

Oxidation of hydrazone **6** to diazo compound **21** was performed with silver oxide and few drops of a saturated solution of potassium hydroxide in methanol.[6] The reaction mixture containing **21** was then filtered[29] at 0°C into a cooled reaction flask and then treated immediately with thioketone **7**. These compounds react in a 1,3-dipolar cycloaddition to give a thiadiazoline, which is unstable and spontaneously extrudes N_2 to give episulfide **22** in 47% yield. Reductive desulfurisation of **22** with copper powder in refluxing *p*-xylene gave alkene **5** in 95% yield. As alkene **5** was obtained as a racemate, HPLC on a chiral stationary phase was performed to resolve a sample to obtain enantiomerically pure (2′*R*)-(*M*)-**5** (configuration determined by X-ray diffraction).

Synthesis of desymmetrized motor by deuteration for studies in solution: In previous studies, unidirectionality of the rotary cycle of related second-generation molecular motors (such as **3**, Figure 2) was confirmed by characterizing each of the stable and unstable isomers in the rotary cycle by ^{1}H NMR spectroscopy.[4] This was made possible by the changes in absorption of the stereogenic methyl substituent in the upper half of the molecule, and of the methoxyl substituents in the lower half. Since the parent motor molecule **5** used in this study appears as two pairs of identical isomers in the four-step cycle, it was necessary to desymmetrize the lower half by introducing an additional spectroscopic handle, here a OCD_3 moiety to replace one of the OCH_3 groups. In contrast to desymmetrizing the lower half by introduction of an additional functional group, this isotopic substitution has the advantage that the photochemical and thermal properties of the motor should be essentially unaltered in comparison to those of the parent molecule. However, the methoxyl groups in **5** are further from the shielding anisotropy of the naphthalene moiety than they are in **3**, and thus the anticipated difference in their chemical shifts in the *cis* and *trans* isomers is reduced. Additionally, the difference in the absorption of the methoxy signals of the stable and unstable forms was expected to be negligible.

Therefore, the unidirectionality of the rotary cycle must be demonstrated by comparing the extent of photoconversion of molecules to the unstable isomer with the extent of isomerisation of the overcrowded alkene. Both can be determined by ^{1}H NMR spectroscopy; the extent of photoconversion of stable to unstable isomer can be measured by determining the absorptions from the methyl substituents at the stereogenic centre, while the extent of isomerisation of the central olefin can be measured by means of the change in the position of the absorption from the OMe group in the lower half of the molecule. If the ratio of stable to unstable matches that of the material that underwent double-bond isomerisation, the process is unidirectional. Thus, the next stage of the project was to synthesize an analogue of **5** in which one of the two CH_3 moieties is replaced by a CD_3 group, as in alkene **38**.

The synthesis of **38** benefits from the approach used in the shorter, higher yield synthesis of thioxanthene lower half **15** (Scheme 3). Clearly, the diastereomers must be separated prior to introduction of the CD_3 group, preferably late in the synthesis to minimize undesired photoisomerisation. To allow subsequent introduction of this CD_3 group in the last step, the motor molecule was desymmetrized by replacing one of the two methoxyl groups with a methoxymethyl ether (MOM) protecting group.

Synthesis of the desymmetrized lower-half ketone (Scheme 5) begins with treating MOM-protected phenol[30] **23** with *n*-butyllithium, followed by elemental sulfur to give thiophenol **24** in 79% yield. This thiophenol was then oxi-

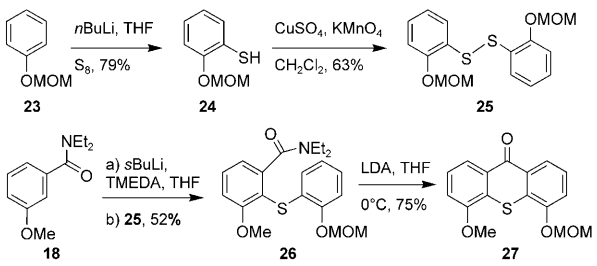

Scheme 5. Synthesis of dissymmetric thioxanthone lower half **27**.

dized to disulfide **25** by using the same procedure as used to prepare **16**.[26] The lithium salt of **18** was then treated with disulfide **25** to provide amide **26**, which was then cyclized by the Snieckus protocol to yield dissymmetric ketone **27**.

The MOM group was hydrolyzed under acidic conditions, and the corresponding phenol **28** then reprotected with benzoyl chloride or acetyl chloride to give ester **29** or **30** in 78 or 50% yield, respectively (Scheme 6). The ketone moieties

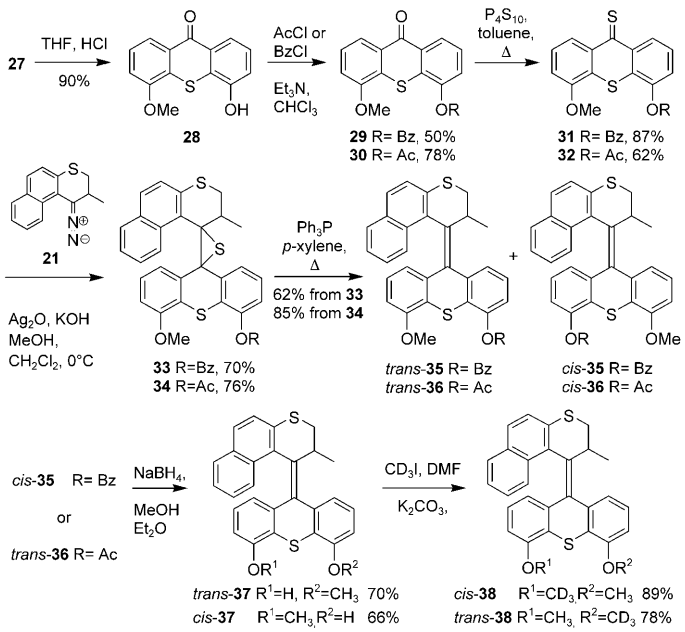

Scheme 6. Synthesis of ^{2}H-labelled molecular motor **38**.

were converted to the corresponding thioketones by heating with P_2S_5 in toluene to give **31** and **32** in 87 and 62% yield, respectively. As both thioketones degraded slowly, they were directly treated with diazo compound **21** to give episulfides **33** and **34** as a mixture of *cis* and *trans* isomers. In contrast to the majority of structurally related episulfides,[4,5,6,8] desulfurisation of **33** and **34** did not proceed readily with copper powder in refluxing toluene. However, they were effectively desulfurized by triphenylphosphine to give **35** and **36**, respectively, as a mixture of diastereomers.

The *cis* and *trans* isomers of benzoyl-protected alkene **35** were inseparable by flash chromatography. The only method we found for separation of these diastereomers employed chiral HPLC, which was impractical to perform on a preparative scale.[31]

Similar difficulties were encountered with the *cis* and *trans* isomers of acetyl-protected alkene **36**. Here, *cis*-**36**[32] proved to be the more soluble of the two diastereoisomers. Unfortunately, the maximum enrichment that could be obtained of either isomer of the alkenes reflected a diastereomeric purity of about 80%, so these isomerically enriched *cis*- and *trans*-alkenes **36** were used in subsequent synthesis and experiments. For *trans*-**36** a sample was obtained containing *trans*-**36** and *cis*-**36** in a ratio of 83:17, and for *cis*-**36** a sample with *cis*-**36**:*trans*-**36** ratio of 80:20 was used. The ester moieties on both isomers were removed by reduction with $NaBH_4$ to provide acceptable yields of *cis*- and *trans*-**37**. Upon deprotonation by K_2CO_3, the phenol groups in both stereoisomers reacted readily with [D_3]methyl iodide in DMF to give deuterium-substituted molecular motors *cis*-**38** and *trans*-**38**. Since isomerically enriched samples were used for the synthesis, *trans*-**38** contained 17% of the *cis* isomer, and *cis*-**38** 20% of the *trans* isomer. The assignment of the configuration (*cis* or *trans*) of the diastereoisomers of **38** were confirmed by comparison of their ^{1}H NMR spectra with that of **5**.

Synthesis of enantiopure motors on gold nanoparticles ((2′*R*)-(*M*)-4): The aliphatic tethers required to anchor the motor molecule to the surface of the nanoparticle were introduced in a six-step procedure, which was followed by enantioresolution of intermediate **43** by HPLC on a chiral stationary phase[33] (Scheme 7). The surprising robustness of motor molecule **5** allowed the methoxyl groups to be deprotected cleanly by treatment with boron tribromide to give bis-phenol **39**.[34]

Alkylation of **39** with two equivalents of monotosylate **40** gave diol **41** in 86% yield.[35,36] Conversion of both of the terminal alcohol moieties of **41** to the corresponding tosylates to give **42** was followed by their displacement by potassium thioacetate to provide **43** in 79% yield over the two steps.

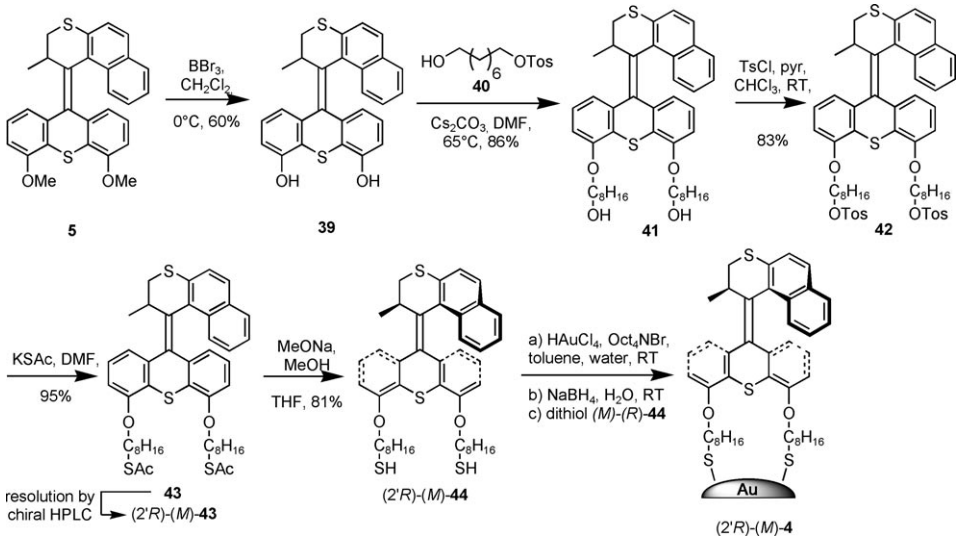

Scheme 7. Functionalisation of the motor molecule and anchoring onto the surface of gold colloidal particles.

Fortunately, at this advanced stage of the synthesis, the enantiomers of **43** could be separated by preparative HPLC on a chiral stationary phase. By comparison of the CD spectra of the first-eluting enantiomer of **43** and (2′*R*)-(*M*)-**5**, the absolute configurations of the enantiomers of **43** were assigned and the synthesis continued with (2′*R*)-(*M*)-**43**. Deprotection of the thiol by treatment with sodium methoxide in a mixture of THF and methanol gave dithiol (2′*R*)-(*M*)-**44**, which was immediately used in the Brust–Schiffrin method for the preparation of small gold nanoparticles.[37] Despite the small scale on which this preparation was performed, the reaction proceeded analogously to those described in the literature to give motor-substituted colloids (2′*R*)-(*M*)-**4**.[38] These colloids were purified by twice inducing their precipitation from toluene by adding methanol. Their ^{1}H NMR spectrum in [D$_8$]toluene showed very broad signals, and no resonances associated with motor molecules that were free in solution were observed.

The UV/Vis spectrum of free motor **5** in solution was compared with that of its gold-attached counterpart (2′*R*)-(*M*)-**4** (Figure 3). The UV/Vis spectrum of nanoparticles protected with octanethiol[15,39] was used as a control to allow us to compensate for the absorption spectrum of the gold core. Thus, the UV/Vis spectrum of nanoparticles protected with octanethiol was subtracted from that of (2′*R*)-(*M*)-**4** to approximate the UV/Vis spectrum of the motor molecules alone (while bound to gold). The subtracted spectrum and the spectrum of **5** are an approximate superposition of one another. Some differences between the spectra may be expected, since the use of different thiols as ligands would lead to small differences in the environment of the gold core.[40]

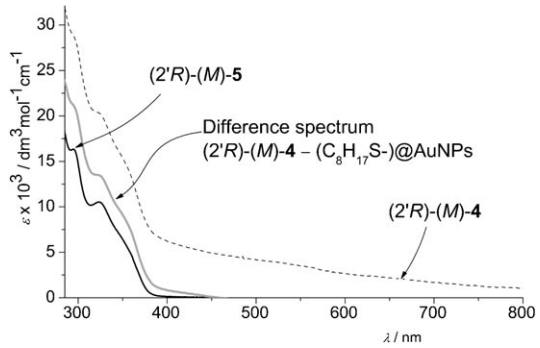

Figure 3. UV/Vis spectra of (2′*R*)-(*M*)-**5** (black, solid), (2′*R*)-(*M*)-**4** (black, dashed) and the difference spectrum of (2′*R*)-(*M*)-**4** versus the UV/Vis spectrum of gold nanoparticles protected with octanethiol (grey).

Synthesis of isotopically labelled motors grafted to gold nanoparticles: To demonstrate unidirectional rotation of motors after grafting to the gold nanoparticles, desymmetrisation of the motor molecule functionalized with eight-carbon "leg" groups could in principle be achieved by deuteration at C1 of the leg (the CH_2 group of the phenol ethers). Our efforts to this end were complicated by the fact that instead of clean singlets (as is observed for OCH_3 in **5**), the two hydrogen atoms of the OCH_2 group are diastereotopic, and thus they show a complex ABXY pattern in which the signals of the stable and the unstable isomers overlap. This made the use of ^{1}H NMR unattractive. As a viable alternative, we introduced a ^{13}C isotopic label at OCH_2 of the linker moiety. Ultimately, this allowed us to verify that the amount of *cis–trans* isomerisation matched the degree of conversion of stable isomer to unstable isomer, consistent with a unidirectional cycle.[13]

Synthesis of ^{13}C-labelled motor **55** required to demonstrate the unidirectional rotary cycle on the nanoparticle (vide supra) started from motor diphenol **39** (Scheme 8). Since it was not obvious which pairs of diastereomers of the synthetic intermediates could be separated, we believed it

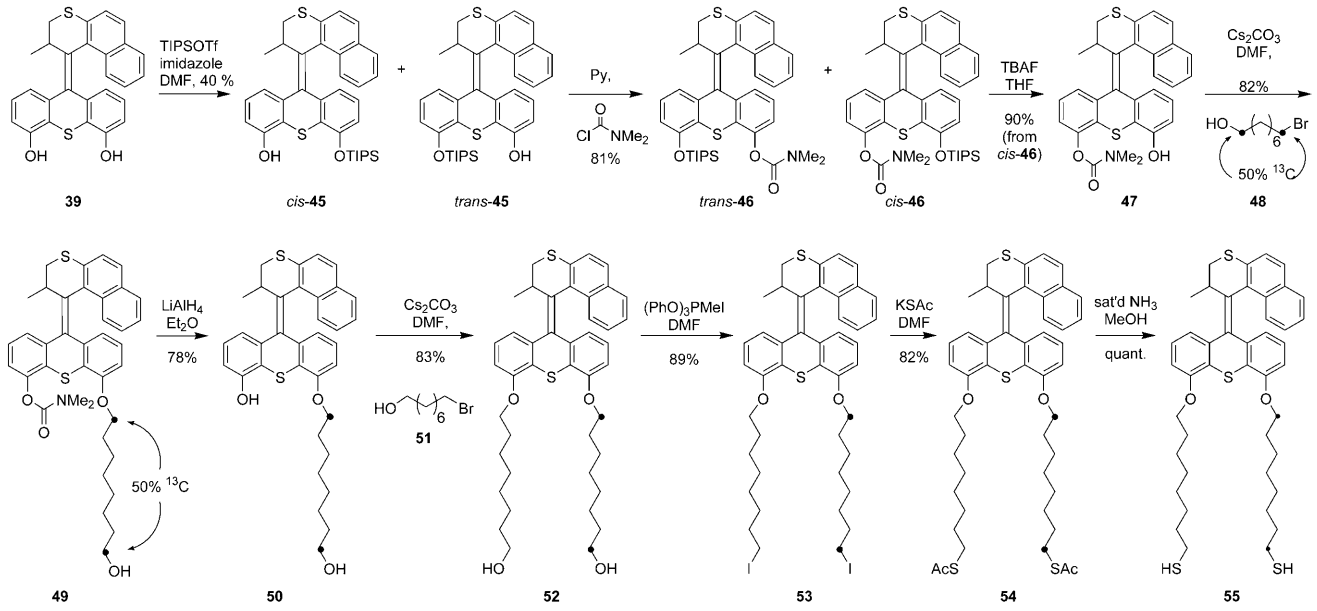

Scheme 8. Preparation of ^{13}C-labelled motor **55** for verification of unidirectionality on the nanoparticle. The black dots denote carbon sites which are enriched to 50 % ^{13}C.

wise to separate the isomers at an earlier stage to avoid a potentially problematic separation in one of the final steps. Additionally, early separation has the practical advantage of making more material available to screen different phenol protecting groups to maximize the chromatographic separation of the diastereomers. The drawback of this approach is that it necessitates handling the material for many synthetic steps under light-reduced conditions to avoid photoisomerisation.

Screening a series of monoprotected derivatives of **39** revealed that introduction of a single hydrophobic triisopropylsilyl (TIPS) group as in **45** gave improved chromatographic separation (Scheme 8).[41] The configuration of the overcrowded alkene was assigned in analogy with the trends in chemical shifts[42] observed for the isomers of **38** and was confirmed by COSY and NOESY spectroscopy.

However, attempts to alkylate *trans*-**45** under a variety of reaction conditions[43] led to scrambling of the TIPS protecting group between the *cis* and *trans* positions and resulted in mixtures of diastereomers of *cis* and *trans* mono- and dialkylated products. The presence of dialkylated (and dihydroxy) product in the mixture excludes simple intramolecular migration of the TIPS group as the only mechanism for this unexpected behaviour. To overcome this scrambling, the remaining free phenoxyl group of a mixture of *cis*- and *trans*-**45** was protected by treatment with *N*,*N*-dimethylcarbamoyl chloride in pyridine to give carbamate *trans*-**46** and *cis*-**46**.

The presence of the dimethyl carbamate increased the difference in R_f of diastereoisomers *trans*-**46** and *cis*-**46** sufficiently to allow their separation by flash chromatography. Thus, the most expedient route to pure desymmetrized material was to carbamoylate the *cis*/*trans* mixture of **45** and then separate the mixture of isomers. Synthesis of the desymmetrized ^{13}C-labelled motor was continued with *cis*-**46**. The TIPS group was cleaved upon treatment with TBAF in 90% yield to give *trans*-**47**. This phenolic compound was alkylated with (50%-$^{13}C_1$/50%-$^{13}C_8$)-8-bromooctan-1-ol[44] (**48**) to give *trans*-**49**. The ^{13}C-labelled C-8 tether was installed first to provide an extremely sensitive way to detect the presence of the other diastereomer. This approach proved useful to ensure the purity of the *trans* diastereomer at every step of the synthesis.[45]

The carbamate protecting group was removed with $LiAlH_4$ in THF to give phenoxy compound **50** in 78% yield, which was then alkylated with (isotopically unenriched) 8-bromooctan-1-ol[46] (**51**) in DMF with Cs_2CO_3 to give **52** in 83% yield. This diol was transformed to diiodide **53** in 89% yield by treatment with triphenoxyphosphonium iodide in DMF.[47] The diiodide was then treated with KSAc at 50°C to afford bis-thioacetate **54** in 82% yield. Dithioester **54** was deprotected with saturated NH_3 in MeOH, which smoothly afforded dithiol **55**.[48] As before, this deprotection was performed immediately prior to preparation of the gold colloids to avoid oxidation of the thiol moieties by atmospheric oxygen.

As with (2′*R*)-(*M*)-**4**, the gold colloids decorated with molecular motor with ^{13}C-labelled legs **55** were prepared by the Brust–Schiffren procedure.[15] These colloids were purified by precipitation from toluene/methanol (2×), followed by size exclusion chromatography on Sephadex LH-20 with $CHCl_3$/MeOH as eluent.[13]

Structural characterisation of model motor 5: To verify that its structure was analogous to those of reported motor molecules derived from overcrowded alkenes, the X-ray structure of **5** was determined (Figure 4a) on crystals of the first-eluted fraction from the enantioseparation of (2′*R*)-(*M*)-**5** and (2′*S*)-(*P*)-**5** (Figure 2) by HPLC on a chiral stationary phase. This confirmed that the methyl substituent (2′ax) at the stereogenic center adopts a pseudo-axial conformation to minimize the steric crowding around the central olefinic bond (C1=C9). Additionally, the substituents attached to the central olefin adopt an *anti*-folded conformation in analogy to reported second-generation molecular motors and related overcrowded alkenes.[6,49] Deviations from planarity are slight (Figure 4c). Ultimately these steric interactions force the molecule to adopt a helical structure, wherein the sign of the helix is dictated by the configuration at the stereogenic center.

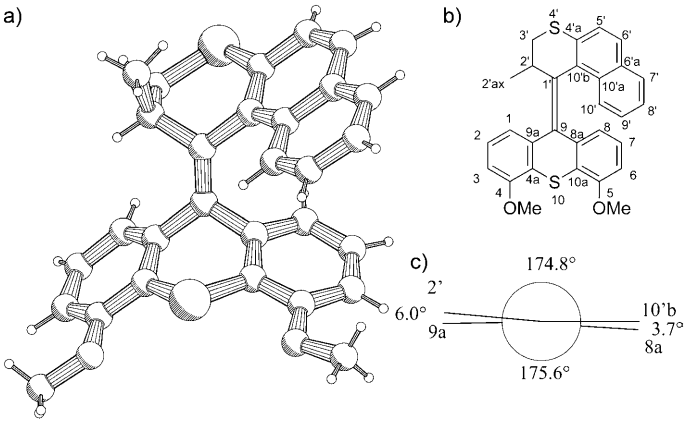

Figure 4. a) Pluto drawing of (2′*R*)-(*M*)-**5** based on the X-ray structure, seen perpendicular to the central alkene. b) Numbering of the molecule. c) Newman projection along the C9=C1 bond.

Since the X-ray structure was obtained on enantiomerically pure material, the Flack refinement[50] [$x = 0.01(5)$] of the crystallographic data allowed the absolute configuration of the first-eluting fraction to be determined as (2′*R*)-(*M*)-**5**.[51,52]

Gold colloids: transmission electron microscopy (TEM) and dynamic light scattering (DLS): Sample substrates for analysis by TEM were prepared by drop-casting dilute solutions of nanoparticles (2′*R*)-(*M*)-**4** in toluene onto an amorphous carbon film (Figure 5). Analysis of 1246 particles gave a mean diameter of 2.01 ± 0.3 nm.

Comparison of the CD spectrum of a solution of (2′*R*)-(*M*)-**4** in toluene with the spectroscopic data obtained for parent compound (2′*R*)-(*M*)-**5** gives the molar quantity of

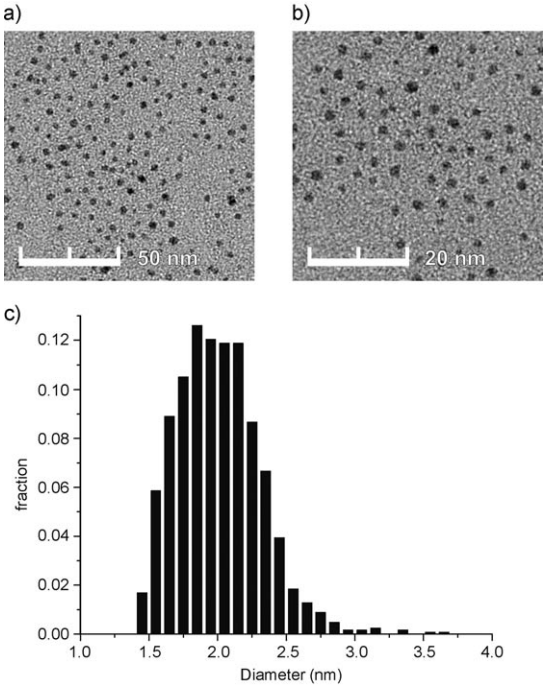

Figure 5. a) and b) Representative transmission electron micrograph of a drop-cast film of (2′*R*)-(*M*)-**4**. c) Size distribution obtained from digital analysis of 1246 nanoparticles.

motor chromophores per gram of nanoparticle. Together with the known particle size (TEM: $d=2.01$ nm) and the density of gold (19.3 g cm^{-3})[53] the number of overcrowded alkenes per nanoparticle was calculated to be approximately 26 ± 2.[54] Since a core diameter of 2.01 nm corresponds to 251 gold atoms, the overall formula of monolayer-protected gold cluster is approximately $Au_{251}\{[S(CH_2)_8O]_2C_{27}H_{18}S_2\}_{26}$.

To determine the size of the functionalized gold colloid particles, DLS measurements were performed at 30.0 °C and $\lambda=633.3$ nm on a solution containing 1 mg of nanoparticles in 1 mL of toluene. Prior to the measurement, the samples were centrifuged for 5 min at 3000 rpm to remove any interfering dust particles from the scattering volume. The intensity autocorrelation functions obtained by DLS were analyzed with CONTIN.[55] The intensity-mean hydrodynamic diameter of the particles was determined to be 6.3 nm. Since the hydrodynamic diameter includes the organic dithiols **44** ligated to the core, this value is close to the expected one: the molecule standing on the particle (approximate height 2.1 nm[56]) in addition to the diameter of the gold core (2.0 nm) would be about 6.2 nm, very close to the observed value.

Analysis of the rotary cycle: step 1 in solution: Using first UV/Vis and CD spectroscopy and then ^{1}H NMR spectroscopy, we show that the rotary cycle of (2′*R*)-(*M*)-**5** is analogous to those of reported rotary molecular motors (Scheme 9). The data obtained from these measurements were then compared with analogous data from motor-decorated gold nanoparticles (2′*R*)-(*M*)-**4**.

*Step 1 of the rotary cycle of **5** monitored by UV/Vis and CD*: First, a solution of (2′*R*)-(*M*)-**5** in toluene (1.69×10^{-5} M) was irradiated with polychromatic light ($T=0$ °C, $\lambda\geq280$ nm), and the changes in the UV/Vis and CD spectra were monitored until no further change occurred, that is, the photostationary state was reached (Figure 6). The major absorption at 283 nm in the CD spectrum changed from positive ($\Delta\varepsilon=+92.6$) to negative ($\Delta\varepsilon=-43.9$), indicative of inversion of the helicity of the molecule. This is consistent with isomerisation of (2′*R*)-(*M*)-**5** to (2′*R*)-(*P*)-**5**. In the UV/Vis spectrum, a decrease in the intensity of the long-wavelength absorption was also consistent with the formation of (2′*R*)-(*P*)-**5**.[57] The clear isosbestic point(s) in both the CD (at $\lambda=305$ nm) and the UV/Vis spectra (at $\lambda=291$, 299, 305, 321 nm) indicated clean photochemical conversion from (2′*R*)-(*M*)-**5** to (2′*R*)-(*P*)-**5**. From the relative absorptions of (2′*R*)-(*M*)-**5** and (2′*R*)-(*P*)-**5** in their UV/Vis spectra, the ideal wavelength for formation of the unstable isomer was determined to be about 365 nm. Irradiation of the sample at this wavelength (mercury line, filter 365 ± 10 nm) indeed resulted in an improved photostationary state consisting of 94% (2′*R*)-(*P*)-**5** and 6% (2′*R*)-(*M*)-**5** (as was determined by ^{1}H NMR spectroscopy in [D$_8$]toluene). This improved photostationary state was also supported by an increase in the intensity of the major CD band at 283 nm ($\Delta\varepsilon=-59.6$) and decrease in the intensity of the absorption at longer wavelength at 347 nm ($\Delta\varepsilon=4000$). The photostationary state ratios determined by ^{1}H NMR spectroscopy (see below) were used to calculate the CD spectrum of pure (2′*R*)-(*P*)-**5**.

*Step 1: photoisomerisation of **5** monitored by ^{1}H NMR spectroscopy*: Formation of (2′*R*)-(*P*)-**5** was confirmed by ^{1}H NMR spectroscopy ([D$_8$]toluene) on a separate (racemic) sample. Three changes in the NMR spectrum are indicative for conversion from stable **5** to unstable **5**.

The doublet for the methyl group adjacent to the stereogenic center shifted downfield from $\delta=0.54$ ppm in stable **5**, in which it occupies a pseudo-axial position, to $\delta=0.90$ ppm

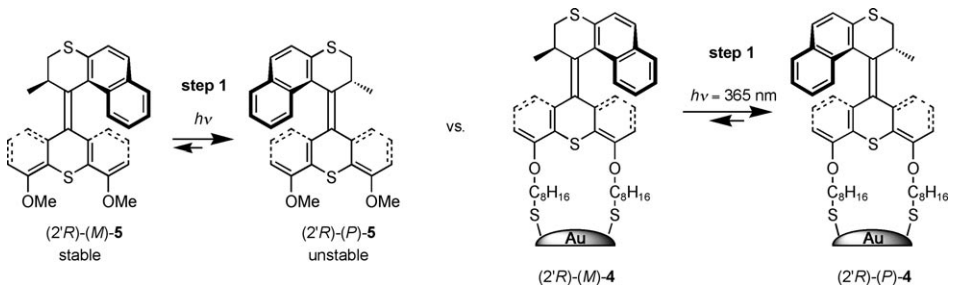

Scheme 9. Step 1 of the rotary cycle of motors in solution and on the nanoparticles.

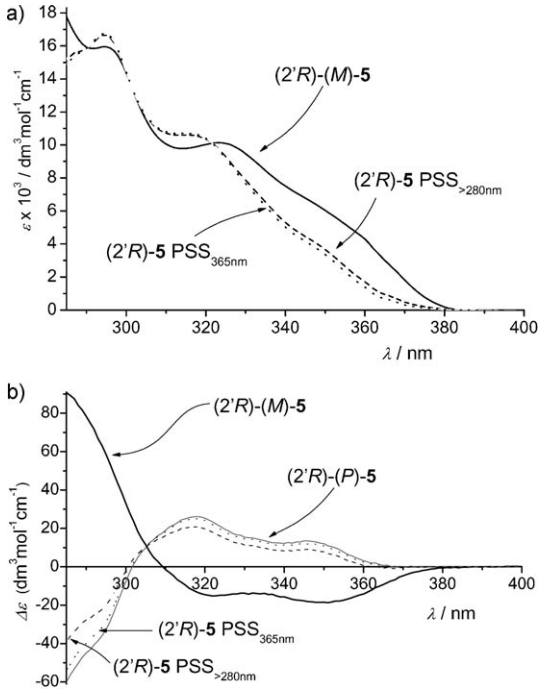

Figure 6. a) UV/Vis spectra of (2′*R*)-(*M*)-**5** (solid), photostationary state ($h\nu = 280$ nm; dashed) and photostationary state ($h\nu = 365$ nm; dotted) in toluene. b) CD spectra of pure (2′*R*)-(*M*)-**5** (solid), $PSS_{280\,nm}$ (dashed), $PSS_{365\,nm}$ (dotted) and the calculated CD spectrum of (2′*R*)-(*P*)-**5** (thick solid, see text for details) recorded in toluene.

in unstable **5**. This shift is due to the increased deshielding experienced by the pseudo-equatorial methyl group in the unstable isomer because of its proximity to the lower-half arene moiety and confirms the conformational change from a pseudo-equatorial to a pseudo-axial orientation. The signals from the aliphatic protons in the upper half changed from $\delta = 4.26$ (m, 1H), 3.58 (m, 1H) and 2.87 ppm (dd, 1H) for stable **5** to $\delta = 3.03$ (overlapping m, 2H) and 2.27 ppm (m, 1H). The shift of the methoxyl protons is small and the signals are poorly resolved. Most of the aromatic signals overlap; the only clear change in the aromatic region is an upfield shift of the doublet at $\delta = 7.88$ ppm for stable **5** to $\delta = 7.73$ ppm for unstable **5**. Comparison of the relative integrations of the signals from the stereogenic methyl groups in the ^{1}H NMR spectrum showed that the photostationary state when irradiated with UV light with $\lambda > 280$ nm contained 91% unstable **5** and 9% stable **5**.

Analysis of the rotary cycle: step 1 on nanoparticles: Using UV/Vis and CD spectroscopies we show that the photochemical step in the rotary cycle of (2′*R*)-(*M*)-**4** is analogous to what we observed with (2′*R*)-(*M*)-**5** (Scheme 9).

Step 1: photoisomerisation of (2′R)-4 monitored by UV/Vis and CD spectroscopy: The photoisomerisation step of motors grafted to gold nanoparticles were studied in toluene solution at room temperature, in analogy with (2′*R*)-(*M*)-**5**. A 1.04×10^{-5} M solution (chromophore concentration)[58] of (2′*R*)-(*M*)-**4** in toluene was irradiated at $\lambda \geq 280$ nm. The UV/Vis and CD spectra of (2′*R*)-(*M*)-**4** before irradiation (solid black) and the $\lambda \geq 280$ nm photostationary state ($PSS_{\geq 280\,nm}$; dashed black line, reached after irradiation for 30 min) show similar changes to their counterparts in solution (Figure 7). Analogous to **5** in solution, sign inversion of

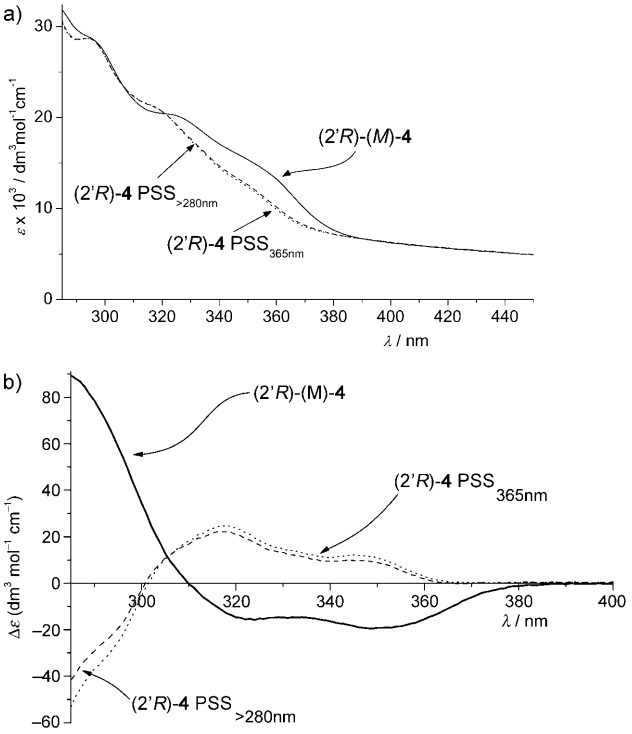

Figure 7. a) UV/Vis spectra of (2′*R*)-(*M*)-**4** (solid), $PSS_{\geq 280\,nm}$ (dashed) and $PSS_{365\,nm}$ (dotted) containing predominantly (2′*R*)-(*P*)-**4** in toluene. All spectra are adjusted for molar concentration of chromophores. b) CD spectra of pure (2′*R*)-(*M*)-**4** (solid), $PSS_{\geq 280\,nm}$ (dashed), and $PSS_{365\,nm}$ (dotted) in toluene; all spectra are adjusted for molar concentration of chromophores for comparison with (2′*R*)-(*M*)-**5**.

the major CD absorption at 283 nm from positive ($\Delta\varepsilon = +91.0$) to negative ($\Delta\varepsilon -46.4$) is indicative of inversion of molecular helicity from (2′*R*)-(*M*)-**4** to (2′*R*)-(*P*)-**4**. In the UV/Vis spectrum a decrease in the intensity of the absorption at 351 nm from $\varepsilon = 15.2 \times 10^3$ to 12.4×10^3 dm^{-1} mol^{-1} cm^{-1} was also consistent with formation of (2′*R*)-(*P*)-**4**. The clear isosbestic point(s) in both the CD spectrum at 305 nm and in the UV/Vis spectrum at 307 and 321 nm indicate clean photochemical conversion from (2′*R*)-(*M*)-**4** to (2′*R*)-(*P*)-**4**. As was observed for parent compound (2′*R*)-(*M*)-**5** in solution, irradiation at 365 nm resulted in more complete photoconversion of (2′*R*)-(*M*)-**4** to (2′*R*)-(*P*)-**4** with concomitant changes in both its UV/Vis and CD spectra.

The composition of the PSS in step 1 comprising (2′*R*)-(*M*)-**4** and (2′*R*)-(*P*)-**4** was estimated by comparing the CD spectra of the motor grafted on nanoparticles with the CD spectra of parent structure (2′*R*)-(*M*)-**5**, for which the PSS was determined by both HPLC and ^{1}H NMR spectroscopy. Examination of the CD spectra show nearly identical absorptions at 317 nm in the CD spectrum of the photostation-

ary state at $\lambda \geq 280$ nm of the nanoparticle solution, for example, $\Delta\varepsilon = +22.2$ at $\lambda = 317$ nm for the PSS of (2′*R*)-**4** versus $\Delta\varepsilon = 20.7$ at $\lambda = 317$ nm for the PSS of (2′*R*)-**5**. This resemblance indicates that the photoequilibrium of the motor mounted on the Au nanoparticle is very similar to that of the free molecule in solution, although some influence of the different chromophore environments (in solution or on Au) on the CD spectra cannot be excluded.[13,17e,f,59] Moreover, we note that the irradiation times required for surface motor chromophores **4** to reach the PSS are more than five times longer than those for an analogous concentration of motor chromophore **5** in solution.

Analysis of the rotary cycle: step 2 in solution: As for step 1, we first used UV/Vis and CD spectroscopy, and then ^{1}H NMR spectroscopy, to show that the rotary cycle of (2′*R*)-(*M*)-**5** is analogous to those of reported rotary molecular motors (Scheme 10). The data obtained from these measurements were then used for comparison with the analogous data from the motor-decorated gold nanoparticles (2′*R*)-(*M*)-**4**.

*Step 2 of the rotary cycle of (2′R)-**5** monitored by UV/Vis and CD spectroscopy*: After (2′*R*)-(*M*)-**5** was irradiated to its $PSS_{365\,nm}$ to generate predominantly (2′*R*)-(*P*)-**5**, it was heated at 70 °C for 2 h, which led to regeneration of the original CD spectrum observed before irradiation. This observation is consistent with complete conversion of (2′*R*)-(*P*)-**5** to stable (2′*R*)-(*M*)-**5**, as a result of the anticipated thermal helix inversion.[6] The kinetics of this thermal helix inversion were examined by CD spectroscopic monitoring of the change in CD intensity at 317 nm with time (Figure 8). From the change in CD with time at various temperatures (50, 60, 70, 80 °C), the rate constant k_t was determined and subsequently used to calculate the Gibbs free energy of activation ($\Delta^{\ddagger}G° = 94 \pm 1$ kJ mol^{-1}), enthalpy of activation ($\Delta^{\ddagger}H° = 27.2 \pm 0.2$ kJ mol^{-1}) and entropy of activation ($\Delta^{\ddagger}S° = -227 \pm 4$ kJ mol^{-1}) by using the Eyring equation. From these parameters it was extrapolated that (2′*R*)-(*P*)-**5** has a half-life of 1.55 h at room temperature (25 °C).

*Step 2 of the rotary cycle of **5** monitored by ^{1}H NMR spectroscopy*: Warming a sample of **5** at its PSS in [D_8]toluene (containing predominantly unstable **5**) to 60 °C for 2 h led to disappearance of the absorptions attributed to unstable **5**, and clean and complete regeneration of the ^{1}H NMR spectrum of stable **5**.

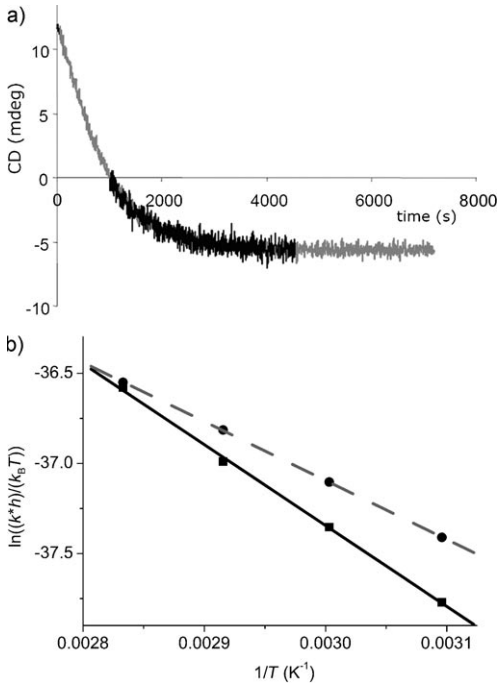

Figure 8. a) CD absorption of irradiated samples containing (2′*R*)-(*M*)-**5** (black) and (2′*R*)-(*M*)-**4** (grey) in toluene at 80 °C, monitored at 316 nm, plotted with respect to time. b) Eyring plot for determination of the Gibbs free energy of activation for helix inversion of (2′*R*)-(*P*)-**4** to (2′*R*)-(*M*)-**4** (grey, dashed) and (2′*R*)-(*M*)-**5** to (2′*R*)-(*P*)-**5** (black, solid). $R^2 > 0.999$ for both plots.

Analysis of the rotary cycle: step 2 on nanoparticles: Using UV/Vis and CD spectroscopy we show that the thermochemical step in the rotary cycle of (2′*R*)-(*M*)-**4** is analogous to that observed for (2′*R*)-(*M*)-**5** (Scheme 10).

*Step 2 of the rotary cycle of (2′R)-**4** monitored by CD and UV/Vis spectroscopy*: Heating a sample of (2′*R*)-**4** at its PSS to 50 °C resulted in restoration of the original CD and UV/Vis spectra. This observation is consistent with quantitative conversion of (2′*R*)-(*P*)-**4** to stable (2′*R*)-(*M*)-**4** by the anticipated thermal helix inversion while grafted to the nanoparticles. As was done for **5**, the kinetics of this thermal helix inversion were examined by CD spectroscopy by monitoring the change in CD intensity at 317 nm with time at various temperatures ($T = 50$, 60, 70, 80 °C). From this data, the rate constant k_t was determined and subsequently used to calculate the Gibbs free energy of activation ($\Delta^{\ddagger}G° = 96 \pm 2$ kJ mol^{-1}), enthalpy of activation ($\Delta^{\ddagger}H° = 37 \pm 1$ kJ mol^{-1}) and entropy of activation ($\Delta^{\ddagger}S° = 200 \pm 4$ kJ mol^{-1}) by

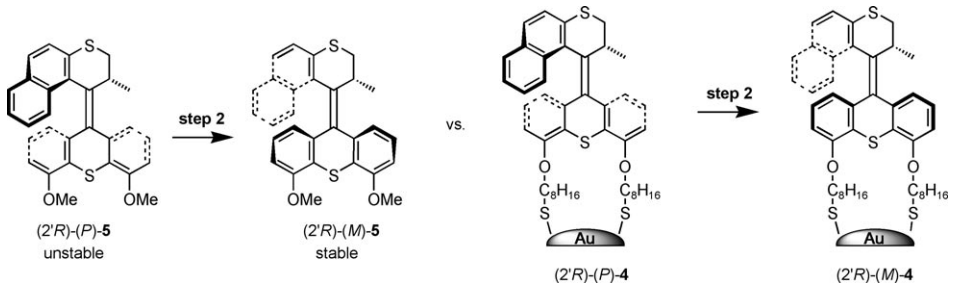

Scheme 10. Step 2 of the rotary cycle of motors in solution and on gold nanoparticles.

using the Eyring equation. This corresponds to a half-life of 3.3 h at room temperature (25 °C) for conversion of (2′*R*)-(*P*)-**4** to (2′*R*)-(*M*)-**4**. This energy barrier is slightly higher than that found for (2′*R*)-(*P*)-**5** and results in an approximate twofold increase of the half-life for thermal helix inversion at room temperature. One possible origin of this slight change in behaviour is the restricted flexibility of the sterically overcrowded alkene when mounted on a gold surface. At elevated temperatures this effect becomes less pronounced, and at 80 °C the half-lives of the thermal helix inversion are very similar: 704 and 725 s for (2′*R*)-(*P*)-**5** and (2′*R*)-(*P*)-**4**, respectively.

^{1}H NMR spectroscopic analysis of deuterated motor 38 to confirm the unidirectional cycle: The photo- and thermal isomerisation processes of **38** were monitored by ^{1}H NMR spectroscopy to verify that its rotary cycle is unidirectional (Figure 9). Comparison of the relative integrals of the diastereomers by ^{1}H NMR spectroscopy confirmed that the cycle is unidirectional, in analogy with related motor molecules.[6,8,60]

Irradiation ($\lambda \geq 280$ nm, $T = 0$ °C) of a sample containing stable *cis*-**38** and stable *trans*-**38** (in 80:20 ratio) in [D_8]toluene led to formation of a photostationary state containing a 91:9 mixture of "total unstable isomers":"total stable isomers", as expected from the analogous experiments performed on non-deuterated motor **5**. The mixture comprised unstable *trans*-**38**, unstable *cis*-**38**, stable *cis*-**38** and stable *trans*-**38** in a ratio of 73:18:7:2, respectively. This ratio of products is consistent with establishment of two separate photo-equilibria: one between unstable *trans*-**38** and stable *cis*-**38** (in a ratio of 73:7, close to 91:9) and the other between unstable *cis*-**38** and stable *trans*-**38** (in a ratio of 18:2, also close to 91:9).

Overnight heating of the photostationary-state sample at 70 °C resulted in complete conversion of unstable *trans*-**38** and unstable *cis*-**38** to stable *trans*-**38** and stable *cis*-**38**, respectively. The ratio of stable *trans*-**38** and stable *cis*-**38** after irradiation and subsequent heating was determined by ^{1}H NMR spectroscopy to be 75:25, which is consistent with isomerisation of the unstable isomers to the corresponding stable isomers. The portion of *trans* isomer (75 %) originates from the sum of the unstable *trans*-**38** (73 %), which isomerizes to the stable form during heating, and the stable isomer already present at the photoequilibrium (an additional 2 %). Similarly, the 25 % of the *cis* isomer originates from the sum of the unstable *cis*-**38** (18 %), which isomerizes to the stable form during heating, and the stable isomer already present in the PSS (an additional 7 %).

The same irradiation experiment was performed on a sample composed of 83 % stable *trans*-**38** and 17 % stable *cis*-**38**. After irradiation ($\lambda \geq 280$ nm, $T = 0$ °C) a mixture was obtained containing unstable *cis*-**38**, unstable *trans*-**38**, stable *trans*-**38** and stable *cis*-**38** in a ratio of 76:15:7:2. Heating ($T = 70$ °C) of this sample also resulted in complete conversion of unstable *cis*-**38** and unstable *trans*-**38** to stable *cis*-**38** and stable *trans*-**38**, which were obtained in a ratio of 78:22.

By means of these two experiments the full rotary cycle was demonstrated (Figure 9). Either stable isomer of **38** can be converted in 91 % selectivity in a photochemical step followed by a thermal step resulting in the formation of the other stable isomer of **38**. During this process, the respective intermediate unstable isomers of **38** are readily detected, which confirms the unidirectionality of the rotary process around the central double bond. Since the difference between a protonated or a deuterated methoxy substituent is not significant in these types of *cis*→*trans* photo-isomerisation processes, the unidirectionality of rotation of isotopically labelled **38** also demonstrates that model motor **38** can undergo unidirectional rotation around the central olefin.

Previously, we reported a detailed study employing ^{13}C-labelled motor **55** grafted to nanoparticles and ^{1}H and ^{13}C NMR spectroscopy to demonstrate that the rotary cycle of the motor attached to the gold colloids (2′*R*)-(*M*)-**4** is unidirectional.[13] We found that the extent of *cis*→*trans* isomerisation was identical to the extent of isomerisation of stable to unstable isomer.[13]

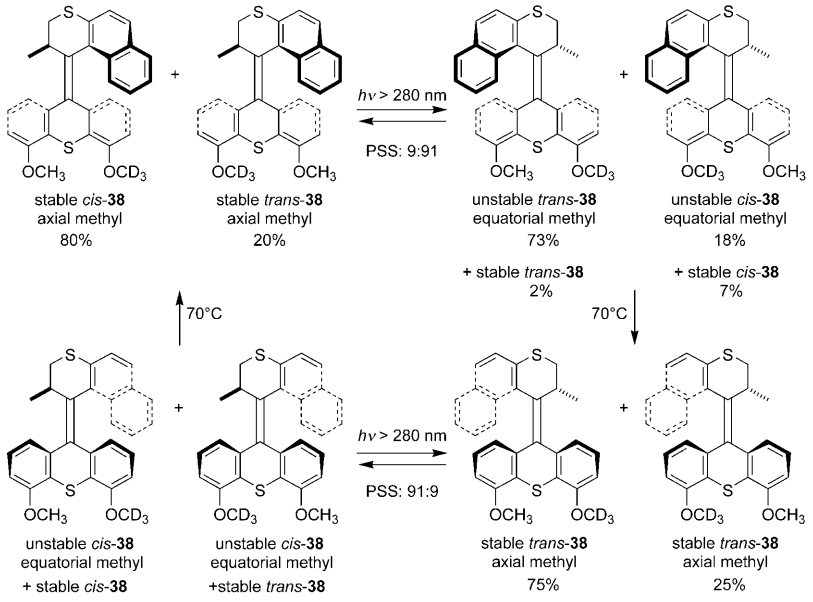

Figure 9. Rotary cycle of deuterated model compound **38**, focussing on the first photochemical and thermal steps for clarity.

Conclusion

We have reported the synthesis of a deuterium-labelled molecular motor and a ^{13}C-labelled molecular motor. These isotopically labelled molecules were essential to demonstrate that the unidirectional rotary cycle of a light-driven rotary molecular motor was preserved when grafted to the surface of a gold nanoparticle. Thus, we have shown that rotation of the upper half relative to the lower half is effectively translated to absolute rotation of the "rotor" with respect to the gold nanoparticle.

Although the motors are each anchored onto the surface through two tethers, the molecules have essentially the same photophysical behaviour as the model motors that function in solution. Comparison of the UV/Vis and CD spectroscopic data obtained for free molecular motors in solution ((2′*R*)-(*M*)-**5**) and when anchored to gold nanoparticles ((2′*R*)-(*M*)-**4**) indicate that the photoequilibria are similar, while the thermal isomerisation step is retarded slightly below 80 °C. Using ^{1}H and ^{13}C NMR spectroscopy on isotopically labelled compounds, we were able to show unequivocally that unidirectionality of rotation is preserved for surface-anchored motor molecules. We anticipate that this work is a promising step toward harnessing the unique molecular-scale controlled rotary motion generated by these motors.[9]

Experimental Section

Experimental procedures and characterisation for all new compounds, including copies of their ^{1}H and ^{13}C NMR spectra and TEM data for (2′*R*)-(*M*)-**4**, are provided in the Supporting Information.

Acknowledgements

Financial support from the Netherlands Organisation for Scientific Research (NWO-CW) through a NWO-CW Top-grant, Spinoza grant from NWO and a Nanoned grant is gratefully acknowledged. J. Vicario thanks the Departamento de Educación, Universidades e Investigación del Gobierno Vasco for a postdoctoral fellowship.

[1] F. Diederich, *Angew. Chem.* **2007**, *119*, 68; *Angew. Chem. Int. Ed.* **2007**, *46*, 68.

[2] R. D. Astumian, *Phys. Chem. Chem. Phys.* **2007**, *9*, 5067.

[3] For progress on molecular motors at work, see a) W. R. Browne, B. L. Feringa, *Nature Nanotech.* **2006**, *1*, 25; b) for a comprehensive review, see: E. R. Kay, D. A. Leigh, F. Zerbetto, *Angew. Chem.* **2007**, *119*, 72; *Angew. Chem. Int. Ed.* **2007**, *46*, 72; c) recent review: B. L. Feringa, *J. Org. Chem.* **2007**, ***72***, 6635; d) V. Balzani, A. Credi, M. Venturi, *ChemPhysChem* **2008**, *9*, 202.

[4] a) N. Koumura, R. W. J. Zijlstra, R. A. van Delden, N. Harada, B. L. Feringa, *Nature* **1999**, *401*, 152; b) M. K. J. ter Wiel, R. A. van Delden, A. Meetsma, B. L. Feringa, *J. Am. Chem. Soc.* **2005**, *127*, 14208.

[5] a) M. K. J. ter Wiel, R. A. van Delden, A. Meetsma, B. L. Feringa, *J. Am. Chem. Soc.* **2003**, *125*, 15076; b) T. Fujita, S. Kuwahara, N. Harada, *Eur. J. Org. Chem.* **2005**, 4533; c) S. Kuwahara, T. Fujita, N. Harada, *Eur. J. Org. Chem.* **2005**, 4544.

[6] a) N. Koumura, E. M. Geertsema, A. Meetsma, B. L. Feringa, *J. Am. Chem. Soc.* **2000**, *122*, 12005; b) N. Koumura, E. M. Geertsema, M. B. van Gelder, A. Meetsma, B. L. Feringa, *J. Am. Chem. Soc.* **2002**, *124*, 5037.

[7] Motor systems driven by chemical transformations: a) S. P. Fletcher, F. Dumur, M. M. Pollard, B. L. Feringa, *Science* **2005**, *310*, 80; b) Y. Lin, B. J. Dahl, B. P. Branchaud, *Tetrahedron Lett.* **2005**, *46*, 8359–8362; c) B. J. Dahl, B. P. Branchaud, *Org. Lett.* **2006**, *8*, 5841; d) T. R. Kelly, H. De Silva, R. A. Silva, *Nature* **1999**, *401*, 150; e) T. R. Kelly, X. Cai, F. Damkaci, S. B. Panicker, B. Tu, S. M. Bushell, I. Cornella, M. J. Piggott, R. Salives, M. Cavero, Y. Zhao, S. Jasmin *J. Am. Chem. Soc.* **2007**, *129*, 376.

[8] M. M. Pollard, M. Klok, D. Pijper, B. L. Feringa, *Adv. Funct. Mater.* **2007**, *17*, 718.

[9] M. M. Pollard, M. Lubomska, P. Rudolf, B. L. Feringa, *Angew. Chem.* **2007**, *119*, 1278; *Angew. Chem. Int. Ed.* **2007**, *46*, 1300.

[10] For selected examples, see a) J. Berna, D. A. Leigh, M. Lubomska, S. M. Mendoza, E. M. Pérez, P. Rudolf, G. Teobaldi, F. Zerbetto, *Nat. Mater.* **2005**, *4*, 704; b) T. D. Nguyen, H.-R. Tseng, P. C. Celestre, A. H. Flood, Y. Liu, J. F. Stoddart, J. I. Zink, *Proc. Natl. Acad. Sci. USA* **2005**, *102*, 10029; c) Y. Liu, A. H. Flood, P. A. Bonvallet, S. A. Vignon, B. H. Northrop, H.-R. Tseng, J. O. Jeppesen, T. J. Huang, B. Brough, M. Baller, S. Magonov, S. D. Solares, W. A. Goddard, C.-M. Ho, J. F. Stoddart, *J. Am. Chem. Soc.* **2005**, *127*, 9745.

[11] N. H. Katsonis, M. Lubomska, M. M. Pollard, B. L. Feringa, P. Rudolf, *Prog. Surf. Sci.* **2007**, *82*, 407.

[12] *Molecular Motors*, (Ed.: M. Schliwa), Wiley-VCH, Weinheim, Germany, **2003**.

[13] For a preliminary report on this work, see: R. A. van Delden, M. K. J. ter Wiel, M. M. Pollard, J. Vicario, N. Koumura, B. L. Feringa, *Nature* **2005**, *437*, 1337.

[14] Three-dimensional models for **3** through its rotary cycle can be found in ref. [6].

[15] a) M. Brust, M. Walker, D. Behell, D. J. Schiffrin, R. Whyman, *J. Chem. Soc. Chem. Commun.* **1994**, 801; b) M.-C. Daniel, D. Astruc, *Chem. Rev.* **2004**, *104*, 293.

[16] P. V. Kamat, *J. Phys. Chem. B* **2002**, *106*, 7729.

[17] a) J. Zhang, J. K. Whitesell, M. A. Fox, *Chem. Mater.* **2001**, *13*, 2323; b) J. Zhang, J. K. Whitesell, M. A. Fox, *J. Phys. Chem. A* **2003**, *107*, 6051; c) T. Kudernac, S. J. van der Molen, B. J. van Wees, B. L. Feringa, *Chem. Commun.* **2006**, 3597; d) A. Manna, P-L. Chen, H. Akiyama, T-X. Wei, K. Tamada, W. Knoll, *Chem. Mater.* **2003**, *15*, 20; e) J. H. Hu, F. Liu, K. Kittredge, J. K. Whitesell, M. A. Fox, *J. Am. Chem. Soc.* **2001**, *123*, 1464; f) S. D. Evans, S. R. Johnson, H. Ringsdorf, L. M. Williams, H. Wolf, *Langmuir* **1998**, *14*, 6436; g) M. O. Wolf, M. A. Fox, *Langmuir* **1996**, *12*, 955.

[18] a) D. H. R. Barton, B. J. Willis, *J. Chem. Soc. Perkin Trans. 1* **1972**, 305; b) R. M. Kellogg, S. Wassenaar, J. Buter, *Tetrahedron Lett.* **1970**, *11*, 4689; c) R. M. Kellogg, S. Wassenaar, *Tetrahedron Lett.* **1970**, *11*, 1987; d) R. M. Kellogg, *J. Org. Chem.* **1972**, *37*, 4045; e) D. H. R. Barton, B. J. Willis, *J. Chem. Soc. Chem. Commun.* **1970**, 1225; f) R. M. Kellogg, *Tetrahedron* **1976**, *32*, 2165; g) J. Buter, S. Wassenaar, R. M. Kellogg, *J. Org. Chem.* **1972**, *37*, 4045.

[19] The Barton–Kellogg reaction was first developed by Staudinger and Siegwart: a) H. Staudinger, J. Siegwart, *Helv. Chim. Acta* **1920**, *3*, 833. The reaction was later explored by A. Schönberg et al.; for leading references see: b) A. Schönberg, D. Cernik, W. Urban, *Ber. Dtsch. Chem. Ges. B* **1931**, *64*, 2577; c) A. Schönberg, E. Frese, *Chem. Ber.* **1968**, *101*, 701.

[20] H. H. Hodgson, *Chem. Rev.* **1947**, *40*, 251.

[21] J. Lindley, *Tetrahedron* **1984**, *40*, 1433.

[22] G. Vasiliu, N. Rasanu, O. Maior, *Rev. Chim.* **1968**, *19*, 561, *Chem. Abstr.* **1969**, *71*, 38739.

[23] a) R. J. Mills, N. J. Taylor, V. Snieckus, *J. Org. Chem.* **1989**, *54*, 4372; b) M. C. Whisler, S. MacNeil, V. Snieckus, P. Beak, *Angew. Chem.* **2004**, *116*, 2256; *Angew. Chem. Int. Ed.* **2004**, *43*, 2206.

[24] This compound has been reported in the literature, but no experimental details were provided: P. Grammaticakis, *Bull. Soc. Chim. Fr.* **1964**, 924.

[25] P. Beak, R. A. Brown, *J. Org. Chem.* **1982**, *47*, 34.
[26] Disulfides **17** and **25** were prepared by a procedure of N. A. Noureldin, M. Caldwell, J. Hendry, D. G. Lee, *Synthesis* **1998**, 1587. Disulfide **17** has been reported previously: L. Gattermann, *Ber. Dtsch. Chem. Ges.* **1899**, *32*, 1136.
[27] For leading references on this procedure, see: a) J. M. Fu, B. P. Zhao, M. J. Sharp, V. Snieckus, *J. Org. Chem.* **1991**, *56*, 1683; b) M. Gray, B. J. Chapell, N. J. Taylor, V. Snieckus, *Angew. Chem.* **1996**, *108*, 1609; *Angew. Chem. Int. Ed. Engl.* **1996**, *35*, 1558; c) O. B. Familioni, I. Ionica, J. F. Bower, V. Snieckus, *Synlett* **1997**, 1081.
[28] a) J. E. McMurry, *Chem. Rev.* **1989**, *89*, 1513; b) A. Furstner, B. Bogdanovic, *Angew. Chem.* **1996**, *108*, 2582; *Angew. Chem. Int. Ed. Engl.* **1996**, *35*, 2442.
[29] This diazo compound is unstable and begins to undergo side reactions upon warming to room temperature.
[30] ^{1}H and ^{13}C NMR spectroscopic data: R. S. E. Conn, A. V. Lovell, S. Karaday, L. M. Weinstock, *J. Org. Chem.* **1986**, *51*, 4710. First preparation: Breslauer, Pictet, *Ber. Dtsch. Chem. Ges.* **1907**, *40*, 3785.
[31] This method necessitated the use of such an apolar eluent (heptane:*i*PrOH 98:2) that the low solubility of **35** rendered this approach prohibitively time consuming and wasteful of solvent.
[32] This assignment is based on the position of the acetyl moiety relative to the naphthalene moiety in the upper half.
[33] HPLC on a Chiralcel AD column as stationary phase and *n*-heptane:*i*PrOH (49:1) as eluent (1 mL min^{-1}). The elution times of the enantiomers were 12.7/14.9 min.
[34] The relatively low solubility of **39** in common organic solvents made it hard to purify.
[35] Tosylate **40** was prepared by the reaction of tosyl chloride with 1,8-octanediol. Experimental details for its synthesis are given in the Supporting Information.
[36] S. K. Nayak, *Synthesis* **2000**, *11*, 1575.
[37] a) M. Brust, M. Walker, D. Bethell, D. J. Schiffrin, R. Whyman, *J. Chem. Soc. Chem. Commun.* **1994**, 801; b) M. Brust, J. Fink, D. Bethell, D. J. Schiffrin, C. J. Kiely, *J. Chem. Soc. Chem. Commun.* **1995**, 1655. M.-C. Daniel, D. Astruc, *Chem. Rev.* **2004**, *104*, 293.
[38] For the sake of clarity, only one motor is depicted, whereas TEM and DLS data suggest the presence of an average of 26 motors per nanoparticle.
[39] B. S. Zelakiewicz, A. C. de Dios, Y.Y. Tong, *J. Am. Chem. Soc.* **2003**, *125*, 18.
[40] The absorption of gold is quite sensitive to its environment: K. Watanabe, D. Menzel, N. Nilius, H.-J. Freund, *Chem. Rev.* **2006**, *106*, 4301. A. Moores, F. Goettmann, *New J. Chem.* **2006**, *30*, 1121.
[41] Preparative HPLC was still required to access preparative amounts of diastereomerically pure material.
[42] Protons on the aromatic lower half positioned on the same side as the naphthalene moiety are shielded and their signals are shifted upfield.
[43] Typical aprotic conditions were explored, including Cs_2CO_3 in DMF with 8-bromooctan-1-ol or 8-iodooctan-1-ol. Amine bases such as diisopropylethylamine were also employed to no apparent advantage.
[44] Compound **48** was prepared from K^{13}CN and 7-bromooctan-1-ol in five steps. See Supporting Information for synthetic procedures.
[45] The synthesis was performed initially by installing the ^{13}C-labelled linker second. However, when this was performed it was later found that a small amount (ca. 5%) of the material had photoisomerized to the unstable form of the opposite diastereomer, which was not evident from the ^{1}H NMR spectra of the precursor. These intermediates were surprisingly sensitive to light.
[46] B. Maurer, A. Grieder, *Helv. Chim. Acta* **1977**, *60*, 1155.
[47] The iodide was used here because it led to a much cleaner and faster reaction.
[48] When sodium methoxide was used in distilled, degassed methanol, it was found that ca. 10% had nevertheless been oxidized to the disulfide. No disulfide was observed when the ammonia solution was used.
[49] I. Agranat, P. U. Biederman, J. J. Stezowski, *Eur. J. Org. Chem.* **2001**, 15–34.
[50] a) H. D. Flack, *Acta Crystallogr. Sect. A* **1983**, *39*, 876–881; b) H. D. Flack, G. Bernardinelli, *Acta Crystallogr. Sect. A* **1999**, *55*, 908–915.
[51] Crystal data for (2′*R*)-(*M*)-**4**: $C_{29}H_{24}O_2S_2$; $M=468.64$; colorless, parallelpiped; monoclinic; space group $P2_1$ (no. 4); $a=8.9625(6)$, $b=22.785(2)$, $c=11.6435(8)$ Å; $\beta=90.127(1)°$; $V=2377.7(3)$ Å^3; $Z=4$; $\rho_{calcd}=1.309$ g·cm^{-3}; $T=110(2)$ K; $\mu=2.49$ cm^{-1}; number of reflections: 11841; number of refined parameters: 786; final agreement factors: $wR(F^2)=0.0863$, $R(F)=0.0420$, GoF = 1.036. CCDC-693600 contains the supplementary crystallographic data for this paper. These data can be obtained free of charge from The Cambridge Crystallographic Data Centre via www.ccdc.cam.ac.uk/data_request/cif.
[52] This is the first example described in the literature in which the absolute configuration of a second-generation motor molecule has been determined by a method other than CD spectroscopy.
[53] *CRC Handbook of Chemistry and Physics* (Ed. D. R. Lide), CRC Press, Boca Raton, **2003–2004**, *84*, pp. 4–59. We acknowledge that this value may differ (±10%) from the density of gold in the nanoparticle: O. D. Häberlen, S.-C. Chung, M. Stener, N. Rösch; *J. Chem. Phys.* **1997**, *106*, 5189.
[54] Allowing for a possible error in molar CD measurements of ±5%.
[55] S. W. Provencher, *Comput. Phys. Commun.* **1982**, *27*, 229.
[56] Calculated by using a structure of **44** minimized by MM2.
[57] A reduction in the intensity of the long-wavelength absorption was observed upon formation of the unstable isomer of **2**.[6]
[58] Calculated by comparing the intensity of the CD absorption at 317 nm.
[59] A number of authors have reported CD spectra of metal nanoparticles protected with chiral nonracemic ligands, but none have described any effects of macroscopic anisotropy. Selected examples: a) T. G. Schaaff, R. L. Whetten, *J. Phys. Chem. B* **2000**, *104*, 2630; b) C. Gautier, T. Bürgi, *J. Am. Chem. Soc.* **2008**, *130*, 7077; c) M. Tamura, H. Fujihara, *J. Am. Chem. Soc.* **2003**, *125*, 15742; d) H. Yao, K. Miki, N. Nishida, A. Sasaki, K. Kimura, *J. Am. Chem. Soc.* **2005**, *127*, 15536.
[60] The composition of the photostationary state mixture was determined by comparison of the relative integrals of the absorptions of the stable and unstable isomers, specifically by using protons of the methyl substituent at the stereogenic center ($\delta=0.54$ in the stable isomer vs. 0.90 ppm in the unstable isomer) and the aromatic protons at $\delta=7.6$–7.9 ppm to compare the ratio of stable to unstable, and the absorptions of the methoxyl groups to evaluate *cis*:*trans* ratios.

Received: April 30, 2008
Revised: July 31, 2008
Published online: November 13, 2008

